Chinese Chemical Letters 33 (2022) 5169–5173

Contents lists available at ScienceDirect

Chinese Chemical Letters

journal homepage: www.elsevier.com/locate/cclet

Engineering large-scaled electrochromic semiconductor films as reproductive SERS substrates for operando investigation at the solid/liquid interfaces

Lingling Yang[a], Jiuju Feng[e], Jia-Ning Wang[b], Zhida Gao[a], Jingwen Xu[a,*], Ye Mei[b,c,d,*], Yan-Yan Song[a,*]

[a] College of Sciences, Northeastern University, Shenyang 110004, China
[b] State Key Laboratory of Precision Spectroscopy, School of Physics and Electronic Science, East China Normal University, Shanghai 200062, China
[c] NYU-ECNU Center for Computational Chemistry at NYU Shanghai, Shanghai 200062, China
[d] Collaborative Innovation Center of Extreme Optics, Shanxi University, Taiyuan 030006, China
[e] College of Chemistry and Life Sciences, Zhejiang Normal University, Jinhua 321004, China

ARTICLE INFO

Article history:
Received 27 December 2021
Revised 29 January 2022
Accepted 3 March 2022
Available online 7 March 2022

Keywords:
Charge transfer
Electrochromism
Oxygen vacancies
SERS substrate
Solid/liquid interface

ABSTRACT

Although surface-enhanced Raman spectroscopy (SERS) has been applied for gathering fingerprint information, even in single molecule analysis, the decayed Raman signals in aqueous solutions largely obstruct the on-site insight reaction process. In this study, large-scaled semiconductor films with multi-walled (TiO_2/WO_3/TiO_2) nanopore distribution are fabricated by combining electrochemical anodization and sputtering technique, and then employed as the SERS substrates for detection of molecules at the solid/liquid interfaces. Given the remarkably improved electrochromic property of the multi-walled film, such SERS substrates were endowed with tunable oxygen vacancy (V_O) density and distribution *via* simply applying electrochemical bias voltage, which enabled one to achieve an enhanced charge transfer efficiency and thus a remarkably increased Raman signal even in solution. The V_O-rich SERS substrate is highly repeatable, thus providing a reliable platform for *in-situ* monitoring of the target molecules or intermediates at the solid/liquid interfaces.

Titanium oxide (TiO_2), known by its high stability and electronic properties, constitutes a versatile platform in the fields of photocatalysis, energy storage, and biomedical applications [1–3]. Operando monitoring of the reactions on a TiO_2 surface is extremely important for investigating the yields of TiO_2-based photocatalysts. The full understanding of the reactions at the water/TiO_2 interface is crucial for further optimization of TiO_2 based photocatalysts or reactors [4]. However, *in-situ* monitoring of the reactions on the TiO_2 surface, especially on-site reactions, under operando conditions is still a challenge. In that regard, surface-enhanced Raman spectroscopy (SERS) is an ideal analytical technology for ultrasensitive surface chemical analysis [5–8]. For example, SERS was successfully employed by Tian *et al.* to investigate the photoinduced reaction on the solid/gas interface of single-crystal TiO_2 [9]. As a matter of fact, most common TiO_2-based catalysts are generally low-cost polycrystalline composites and TiO_2 nanomaterials are usually applied in a liquid environment. Meanwhile, compared with strong signals from a solid/gas interface, the largely decayed Raman signals in the liquid medium mean that the use of semiconductor-based SERS substrates in practice is difficult [10]. Therefore, improving the SERS activity of semiconductor-based substrate in liquid medium has become an urgent task.

For semiconductor-based SERS substrates, it is generally agreed that the tuning of photoinduced charge-transfer (PICT) through band energy alignment between substrate and molecule plays a dominant role [11]. Till now, lots of strategies have been developed to promote PICT efficiencies, such as n-/p- doping and stoichiometry [12–14]. Especially, injecting oxygen vacancies (V_O) as an important method in stoichiometry has been demonstrated to be useful for providing some additional defect levels in the bandgap of semiconductors, thus facilitating the exciton resonance in semiconductors, as well as the charge transfer (CT) between semiconductors and molecules [15–17]. Recently, the SERS activities of self-organized TiO_2 nanotubes have been discovered by Weidinger and coworkers [18]. Nevertheless, the Raman activity of TiO_2 nanotube arrays is significantly inferior to that of layered two-dimensional

* Corresponding authors.
E-mail addresses: xujingwen@mail.neu.edu.cn (J. Xu), ymei@phy.ecnu.edu.cn (Y. Mei), yysong@mail.neu.edu.cn (Y.-Y. Song).

https://doi.org/10.1016/j.cclet.2022.03.011
1001-8417/

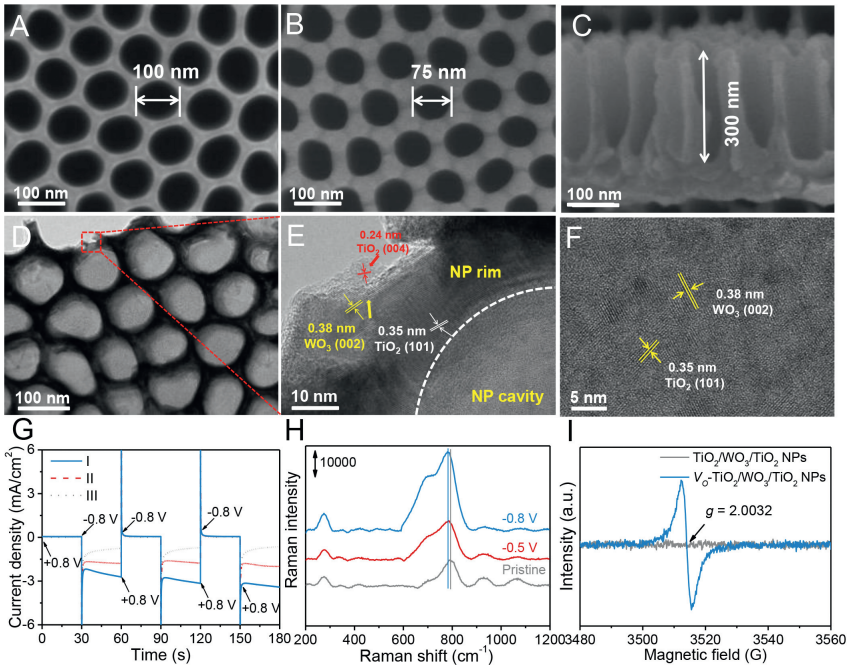

Fig. 1. SEM images of (A) TiO_2NPs and (B, C) $TiO_2/WO_3/TiO_2$NPs. (D) TEM, HAADF-STEM (inset), and (E, F) HR-TEM images of $TiO_2/WO_3/TiO_2$NPs. (G) Current density *vs.* time curves of TiO_2NPs (I), TiO_2/TiO_2NPs (II), and $TiO_2/WO_3/TiO_2$NPs (III) acquired during potential pulse cycling in a voltage range from –0.8 V to +0.8 V. (H) SERS spectra of $TiO_2/WO_3/TiO_2$NPs after applying different bias voltage. (I) EPR spectra of $TiO_2/WO_3/TiO_2$NPs and V_O-$TiO_2/WO_3/TiO_2$NPs.

(2D) semiconductor materials, which have been demonstrated to possess a large number of structural defects [19–21]. Besides the structural defects induced V_O, Zhao and coworkers also utilized electrochromic technology to introduce V_O into the WO_3 substrate [22]. Inspired by the intrinsic electrochromic capacity, feasibility, and widespread applicability of TiO_2 nanopore films (TiO_2NPs) prepared by electrochemical anodization [23,24], we hypothesis that V_O would be also inserted by an electrochromic way, thus enabling TiO_2NPs to be employed as alternative SERS substrates.

For this purpose, we developed a facial and effective approach to prepare a large-scale porous semiconductor substrate with good electrochromic performance. The SERS measurements were carried out by employing bis(tetrabutylammonium) dihydrogen bis(isothi ocyanate) bis(2,2′-bipyridyl-4,4′-dicarboxylate) ruthenium(II) (N719) placed onto $TiO_2/WO_3/TiO_2$NPs. The generation of tunable V_O *via* electrochromic processing of the substrate resulted in the noticeable increase of the Raman signals of N719, and the PICT-mediated signal enhancement was attributed to the V_O induced by electrochromic effect.

The multi-walled NPs were constructed on the self-ordered TiO_2NPs that were prepared by electrochemical anodization. The scanning electron microscopy (SEM) images reveal the uniform nanotube structure of the as-formed TiO_2NPs with the inner diameter of ~100 nm and the length of 300 nm (Fig. 1A and Fig. S1 in Supporting information). The W and Ti nanoparticles were subsequently applied onto the NPs *via* sputtering in sequence. This enabled one to increase the wall thickness and roughness of the NPs (Figs. 1B and C). The final NPs exhibited a smaller inner diameter. The uniform distributions of W and Ti elements across the tube surface and walls were confirmed *via* the morphological and elemental characterization (Fig. S2 in Supporting information), and the structural uniformity of NPs was crucial for obtaining the SERS substrates with good signal reproducibility. The annealing was carried out at 300 °C to achieve the high degree of crystallinity of the hybrid NPs. The X-ray diffraction (XRD) experiments were carried out to demonstrate the annealing-induced crystalline phase transition. After annealing, the peaks attributed to a monoclinic WO_3 phase with preferential (002) orientation (2θ = 23.0°) and anatase TiO_2 with (101) orientation (2θ = 25.3°) could be detected (Fig. S3 in Supporting information). The morphology of $TiO_2/WO_3/TiO_2$NPs was further characterized by transmission electron microscope (TEM) and high resolution (HR)-TEM in Figs. 1D-F and Fig. S4 (Supporting information). The crystal lattices of WO_3 (002) and TiO_2 (101) (004) can be identified at the wall of the resulted sample. These crystalline phases possess high conductivity and cyclic voltammetry stability [24]. The current response and electrochromic switching ability were investigated within a potential window between +0.8 V and −0.8 V (Fig. 1G). The amounts of inserted and extracted electrons during the voltage scanning were calculated based on the current-time curves. The $TiO_2/WO_3/TiO_2$NPs exhibited the charge density $Q_{cathodic}$ of −95.9 mC/cm^2, which was much higher than those of the samples without WO_3 coating (−37.8 mC/cm^2 for TiO_2NPs and −68.5 mC/cm^2 for TiO_2/TiO_2NPs). Noticeably, the insertion of H^+ protons from the electrochromic materials *via* the application of negative bias voltage was accompanied by a reflectance change (Fig. S5 in Supporting information), which could be attributed to the lower valence states of W- and Ti-ions [25]. Clearly, $TiO_2/WO_3/TiO_2$NPs underwent the more pronounced reflectance changes than the other two samples under applying the same bias voltage, and the electrochromic performance can be simply tuned by applying different voltages (Fig. S6 in Supporting information).

The SERS spectra of $TiO_2/WO_3/TiO_2$NPs exposed to various negative bias voltages (labeled as V_O-$TiO_2/WO_3/TiO_2$NPs) are plotted in Fig. 1H. It is worth mentioning that the Raman peaks of WO_3 broaden after the negative bias voltage (−0.5 V and −0.8 V) is applied, which can be explained by the generation of V_O in the substrate [26]. The introduction of V_O in $TiO_2/WO_3/TiO_2$NPs by applying with negative bias voltages was also verified by electron paramagnetic resonance (EPR) spectrum (Fig. 1I), XRD analysis (Fig. S7 in Supporting information), Electrochemical impedance spectroscopy (Fig. S8 in Supporting information), and *in-situ* generation of metal silver (Fig. S9 and Table S1 in Supporting information). It is important to note that plenty of V_O in the SERS substrates are

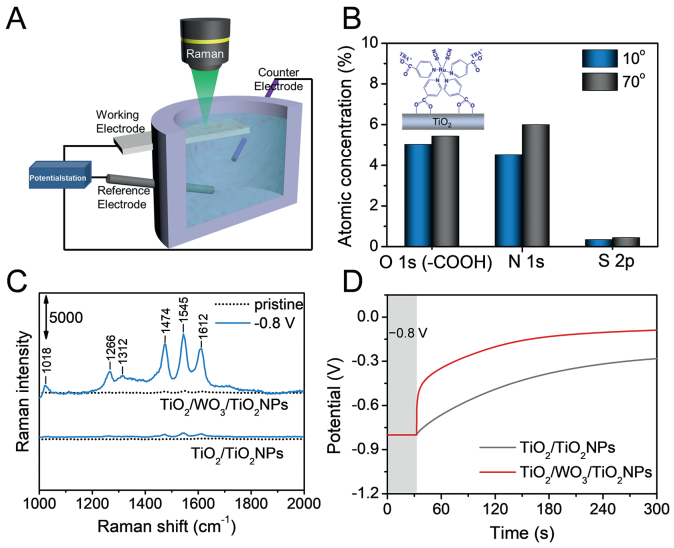

Fig. 2. (A) Schematic of the electrochemical-SERS setup used in this study. (B) Atomic concentrations of N719 modified $TiO_2/WO_3/TiO_2$NPs at take-off angles of 10° and 70° (inset: orientation of N719 on the sample). (C) SERS spectra of N719 (3×10^{-3} mol/L) on pristine and V_O-contained $TiO_2/WO_3/TiO_2$NPs and TiO_2/TiO_2NPs. (D) Potential recovery of TiO_2/TiO_2NPs and $TiO_2/WO_3/TiO_2$NPs after applying the negative bias voltage of −0.8 V for 30 s.

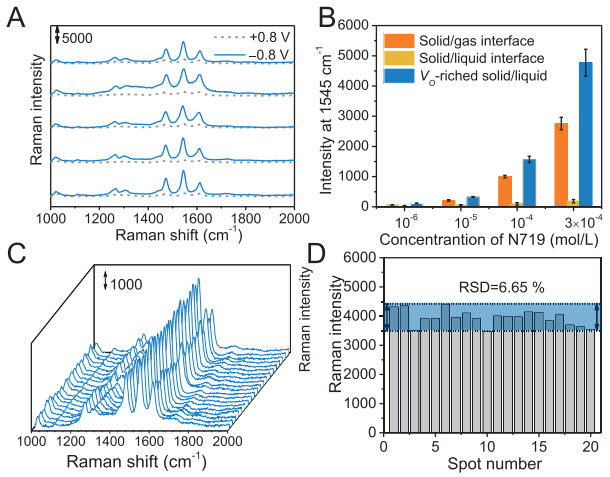

Fig. 3. (A) SERS spectra of N719 adsorbed on $TiO_2/WO_3/TiO_2$NPs after exposed to the bias voltages of −0.8 V and +0.8 V alternately. (B) Raman intensity (at 1545 cm^{-1}) of N719 on $TiO_2/WO_3/TiO_2$NPs measured in air and in liquid. (C) SERS spectra of N719 collected from 20 randomly selected positions on V_O-$TiO_2/WO_3/TiO_2$NPs. (D) Intensity variation of the Raman peak at 1545 cm^{-1} in these 20 selected positions.

conducive thus facilitating the PICT between the probe molecules and the substrates [15]. For semiconductors, the introduction of V_O can bring about a defect state that overlaps with the conduction band (CB), leading to the emergence of a band tail (Fig. S10 in Supporting information) [27]. It is expected that the CT between the substrate and the adsorber would thus be facilitated, and leading to a preferable SERS activity.

As a proof-of-concept, the Raman spectra of N719 onto $TiO_2/WO_3/TiO_2$NPs were *in-situ* collected in HCl electrolyte by using a custom-built electrochemical cell (Fig. 2A). In this study, the NPs samples were exposed to a negative potential for 30 s to introduce V_O in the substrate, and the Raman signals were then acquired at the open circuit potential. Considering the energy match between the incident photons and the absorption spectra of N719 (Fig. S11 in Supporting information), a 532 nm laser was chosen as the excitation light source for the Raman measurements. The orientation of N719 on the TiO_2 surface was investigated using an angle X-ray photoelectron spectroscopy (XPS) at the take off angles θ of 10° and 70° (Fig. S12 in Supporting information). As shown in Fig. 2B and Table S2 (Supporting information), the O 1s (−COOH), N 1s, and S 2p signals exhibit the higher atomic concentrations at 70° (bulk models) than those at 10°. Meanwhile, the atomic population on the N 1s signals at 70° is obviously higher than those on the O 1s (−COOH) and S 2p signals. These results suggest that the −SCN groups are oriented far away from the Raman substrates, and N719 molecules have been anchored onto the TiO_2 surface in the form of a bridged configuration *via* the two carboxyl groups. Such bidentate coordination was considered to provide a favorable way for the CT between the substrate and adsorbed molecules [28]. Compared to the faint signals collected on the pristine samples (see the dot lines in Fig. 2C), the prominent signals of N719 molecules at 1474, 1545, and 1612 cm^{-1}, corresponding to a typical 2,2′-bipyridyl(bpy) ring stretching mode [29], were acquired on the V_O-containing samples (the solid lines in Fig. 2C). In Fig. 2C, V_O-$TiO_2/WO_3/TiO_2$NT exhibits a higher SERS activity than V_O-TiO_2/TiO_2NPs. This phenomenon can be ascribed to the WO_3 thin layer. Owing to the large optical modulation capacity, long-term durability, and memory effect of WO_3, the coating of WO_3 onto TiO_2 can efficiently improve the electrochromic efficiency (Fig. 2D and Fig. S13 in Supporting information). Furthermore, an excessively thick WO_3 film could result in a rough surface and the higher charge-transfer resistance (Figs. S14 and S15 in Supporting information) [30]. Therefore the W-sputtering thickness in this study was optimized at 5 nm (Figs. S16 and S17 in Supporting information).

The role of V_O on the SERS signal of the substrates was further investigated by repeatedly applying positive and negative voltages cycles. In Fig. 3A, an enhanced N719 signal can be observed when applying the voltage of −0.8 V. In turn, switching the voltage to +0.8 V causes the weak Raman signals. The repeatable SERS activities were achieved by switching the voltages back to −0.8 V, verifying the V_O can be electrochemically tuned with satisfactory feasibility and reproducibility. Meanwhile, these results also allow one to conclude whether the weakened SERS activity is derived from the vanishing of V_O rather than from the shedding or desorption of N719 molecules from the substrates.

To evaluate the application advantage of the proposed strategy in aqueous solutions, the Raman signals at 1545 cm^{-1} ($\nu_{(C=C)(bpy)}$, the stretching of the C=C bond in bpy) were collected at different N719 concentrations on $TiO_2/WO_3/TiO_2$NPs in air and in aqueous solution (Fig. 3B). Apparently, the Raman signals recorded in aqueous solution are much weaker than those acquired in air. Impressively, a 39-fold increase in the Raman signals was achieved from the SERS substrates with embedded V_O under a negative bias voltage. Notably, the Raman signals recorded on such a V_O-rich substrate in aqueous solution even exceeded those obtained in air. Moreover, the Raman signal was still conspicuous in the solution when the N719 concentration decreased to 10^{-6} mol/L (Fig. S18 in Supporting information and Fig. 3B), indicating high sensitivity of the V_O-rich substrate. The enhancement factor (EF) of V_O-$TiO_2/WO_3/TiO_2$NPs was calculated to be 8.6×10^4 (Fig. S19 in Supporting information). Additionally, Fig. 3C shows the Raman signals of N719 at twenty randomly selected regions on V_O-$TiO_2/WO_3/TiO_2$NPs. The relative standard deviation (RSD) of the Raman peak at 1545 cm^{-1} is determined to be 6.65% (Fig. 3D), indicating excellent reproducibility of the V_O-rich substrates.

For a comprehensive understanding of the mechanism of V_O-induced SERS activity, the Raman spectra of N719 were investigated under different voltages (Fig. 4A). Owing to the increase in the V_O content with increasing negative bias voltage, the Raman

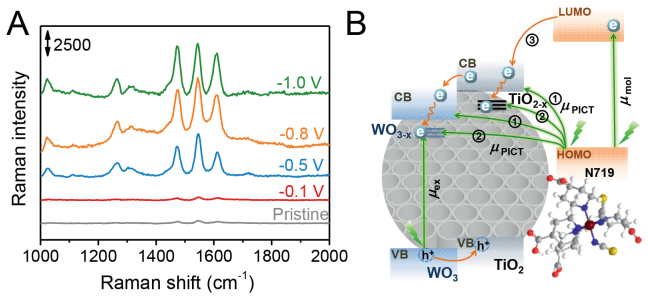

Fig. 4. (A) SERS spectra of N719 on $TiO_2/WO_3/TiO_2$NPs before and after exposure to different bias voltages. (B) Schematic energy level diagram and CT pathways in the N719-V_O-$TiO_2/WO_3/TiO_2$NPs system.

signal intensity from the substrates became substantially higher [26]. The band structural analysis for V_O-$TiO_2/WO_3/TiO_2$NPs and N719 specimens was also carried out at different voltages (Figs. S20 and S21 and Table S3 in Supporting information). Compared to pristine samples, V_O-$TiO_2/WO_3/TiO_2$NPs exhibited the narrower bandgaps. The Mott-Schottky analysis also demonstrates that the charge-carrier density (N_d) calculated for V_O-$TiO_2/WO_3/TiO_2$NPs (3.45×10^{19} cm^{-3}) is larger than that of the pristine sample (1.84×10^{18} cm^{-3}), which is beneficial for the acceleration of PICT in V_O-$TiO_2/WO_3/TiO_2$NPs. Meanwhile, the contribution of CT in V_O-$TiO_2/WO_3/TiO_2$NPs to the SERS signal of N719 was quantifiably determined based on the following equation [16]:

$$\rho_{CT} = \frac{I^k(CT) - I^k(SPR)}{I^k(CT) + I^o(SPR)} \quad (1)$$

According to the SERS spectra in Fig. S22 (Supporting information), the degree of CT (ρ_{CT}) of N719 was calculated as 0.41 and 0.69 for $TiO_2/WO_3/TiO_2$NPs and V_O-$TiO_2/WO_3/TiO_2$NPs, respectively (details were provided in supporting Information). The key role of CT in our system was further demonstrated *via* attaching other Raman probes onto $TiO_2/WO_3/TiO_2$NPs by chemical bonding (4-MBA) or physical absorption ($Ru(bpy)_3^{2+}$ and 2,2′-Bipyridine) (Fig. S23 in Supporting information). Compared to 4-MBA, the SERS signals of $Ru(bpy)_3^{2+}$ and 2,2′-Bipyridine were poor and didnot exhibit obvious enhancement on V_O-$TiO_2/WO_3/TiO_2$NPs. Moreover, the signal of N719 was remarkably dropped when a thin layer of SiO_2 film was covered onto $TiO_2/WO_3/TiO_2$NPs before N719 modification to block CT between substrate and molecules (Figs. S24 and S25 in Supporting information). All these results indicate that CT plays an important role in the improved SERS signals after applying the negative bias.

Considering the location of the highest occupied molecular orbital (HOMO, −5.34 eV) and the lowest unoccupied molecular orbital (LUMO, −3.01 eV) of N719 molecules [31], the PICT could take place in following pathways (Fig. 4B): (1) PICT from the HOMO of N719 to the CB of TiO_2 and WO_3. The electrons can be directly excited from the HOMO of N719 to CB of TiO_2 (−4.21 eV) and WO_3 (−5.24 eV) [32] by an incident light of 532 nm (2.33 eV). (2) PICT from the HOMO of N719 to the defect levels (TiO_{2-x} and WO_{3-x}). In general, the defect levels induced by V_O are usually located at ~0.5−1.0 eV below the minimum value of CB [33]. As a result, PICT from HOMO of N719 to defect levels (TiO_{2-x} and WO_{3-x}) can provide more available PICT pathways than the sample that only contains TiO_2 and WO_3, which can further lead to a magnification of the Raman scattering cross section, thus greatly magnifying the polarization tensor of N719 molecules. (3) Electrons in the LUMO of N719 transfer from the photo-excited N719 molecules to CB of TiO_2. In addition, because of the existence of the defect levels (WO_{3-x}), the band gap of WO_3 can be narrowed as 1.7−2.2 eV [33]. Therefore, electrons can be excited from VB to WO_{3-x} (μ_{ex}) by a 532-nm laser and the photogenerated holes in WO_{3-x} subsequently transfer to VB of TiO_2. Meanwhile, excited electrons in CB of TiO_2 transfer to CB of WO_3. Therefore, a built-in electric field at the interface of TiO_2 and WO_3 with the direction of the electric field pointing from WO_3 to TiO_2 is formed. Driven by the built-in electric field, photogenerated electron-hole pairs can be effectively separated, realizing spatial charge separation and prolongating the lifetime of charge carriers, and thus enhancing the SERS activity [17,34-37].

To summarize, the electrochromic properties of the semiconductors were utilized to successfully produce the highly active SERS substrates that could be applied in aqueous electrolytes. Experiment data and theoretical calculation revealed that the abundant V_O induced by the electrochromic process facilitates the CT between the substrate and adsorbed molecules, thus enhancing their SERS activity. Especially, the as-proposed substrates were largely scalable, and their Raman signals were reproduced by controlling the applied bias voltage, thus providing an easily assessable and low-cost platform for *in-situ* monitoring of the reactions at the solid/liquid interfaces.

Declaration of competing interest

The authors declare that they have no known competing financial interests or personal relationships that could have appeared to influence the work reported in this paper.

Acknowledgments

This work was supported by National Natural Science Foundation of China (Nos. 21874013, 22074013 and 22073030), the Fundamental Research Funds for the Central Universities (Nos. N2105018 and N2005027), and the China Postdoctoral Science Foundation (No. 2019M661109). The CPU time was supported by the Supercomputer Centre of East China Normal University (ECNU Public Platform for Innovation No. 001). Special thanks are due to the instrumental or data analysis from Analytical and Testing Center, Northeastern University.

Supplementary materials

Supplementary material associated with this article can be found, in the online version, at doi:10.1016/j.cclet.2022.03.011.

References

[1] A. Fujishima, K. Honda, Nature 238 (1972) 37–38.
[2] K. Lee, A. Mazare, P. Schmuki, Chem. Rev. 114 (2014) 9385–9454.
[3] C. Zhao, L. Zhou, Z. Zhang, et al., J. Phys. Chem. Lett. 11 (2020) 9931–9937.
[4] X.X. Han, L. Chen, U. Kuhlmann, et al., Angew. Chem. Int. Ed. 126 (2014) 2514–2517.
[5] F. Kruse, A.D. Nguyen, J. Dragelj, et al., J. Am. Chem. Soc. 143 (2021) 2769–2776.
[6] L. Liu, X. Du, Chin. Chem. Lett. 32 (2021) 1942–1946.
[7] D. Buhrke, P. Hildebrandt, Chem. Rev. 7 (2020) 3577–3630.
[8] A.U.R. Bacha, I. Nabi, Z. Fu, et al., Chin. Chem. Lett. 30 (2019) 2225–2230.
[9] S.P. Zhang, J.S. Lin, R.K. Lin, et al., Chem. Sci. 11 (2020) 6431–6435.
[10] L. Yang, C. Zhao, J. Xu, et al., Chem. Commun. 56 (2020) 10333–10336.
[11] S. Schlücker, Angew. Chem. Int. Ed. 53 (2014) 4756–4795.
[12] X. Fan, M. Li, Q. Hao, et al., Adv. Mater. Interfaces 6 (2019) 1901133.
[13] L. Lan, Y. Gao, X. Fan, et al., Front. Phys. 16 (2021) 43300.
[14] I. Alessandri, J.R. Lombardi, Chem. Rev. 116 (2016) 14921–14981.
[15] X. Wang, W. Shi, S. Wang, et al., J. Am. Chem. Soc. 141 (2019) 5856–5862.
[16] G. Song, W. Cong, S. Gong, Z. Zhao, Angew. Chem. Int. Ed. 60 (2021) 5505–5511.
[17] J. Seo, J. Lee, Y. Kim, et al., Nano Lett. 20 (2020) 1620–1630.
[18] I.H. Oer, C.J. Querebillo, C. David, et al., Angew. Chem. Int. Ed. 57 (2018) 7225–7229.
[19] Y. Yang, W. Wei, P. He, et al., Chin. Chem. Lett. 33 (2022) 2600–2604.
[20] Z. Yu, L. Huang, Z. Zhang, G. Li, Chin. Chem. Lett. 33 (2022) 3853–3858.
[21] C. Hess, Chem. Soc. Rev. 50 (2021) 3519–3564.
[22] S. Cong, Z. Wang, W. Gong, et al., Nat. Commun. 10 (2019) 678.
[23] Y.C. Nah, A. Ghicov, D. Kim, S. Berger, P. Schmuki, J. Am. Chem. Soc. 130 (2008) 16154–16155.

[24] Y.Y. Song, Z.D. Gao, J.H. Wang, X.H. Xia, R. Lynch, Adv. Funct. Mater. 21 (2011) 1941–1946.
[25] K. Chang, X. Hai, J. Ye, Adv. Energy Mater. 6 (2016) 1502555.
[26] G. Wang, Y. Ling, H. Wang, et al., Energy Environ. Sci. 5 (2012) 6180–6187.
[27] X. Chen, L. Liu, P.Y. Yu, S.S. Mao, Science 331 (2011) 746–750.
[28] T. Pan, G. Song, S. Cong, et al., J. Phys. Chem. C 124 (2020) 20530–20537.
[29] Z. Mao, Y. Ye, H. Lv, et al., Angew. Chem. Int. Ed. 59 (2020) 10780–10784.
[30] M. Altomare, N.T. Nguyen, S. Hejazi, P. Schmuki, Adv. Funct. Mater. 28 (2018) 1704259.
[31] X. Yang, Y. Chen, P. Liu, et al., Adv. Funct. Mater. 30 (2020) 2001557.
[32] H. Zhu, Q. Yang, D. Liu, et al., J. Am. Chem. Soc. 143 (2021) 9236–9243.
[33] Z. Zheng, S. Cong, W. Gong, et al., Nat. Commun. 8 (2017) 1993.
[34] M. Li, X. Fan, Y. Gao, T. Qiu, J. Phys. Chem. Lett. 10 (2019) 4038–4044.
[35] M. Li, Y. Wei, X. Fan, et al., Nano Res. 15 (2022) 637–643.
[36] X. Fan, P. Wei, G. Li, et al., ACS Appl. Mater. Interfaces 13 (2021) 51618–51627.
[37] J. Seo, J. Lee, Y. Kim, et al., Nano Lett. 20 (2020) 1620–1630.